CrystEngComm

Control of Location and Distribution of Heteroatoms Substituted Isomorphously in Framework of Zeolites and Zeotype Materials

Journal:	*CrystEngComm*
Manuscript ID	CE-HIG-07-2021-000912.R1
Article Type:	Highlight
Date Submitted by the Author:	10-Aug-2021
Complete List of Authors:	Yabushita, Mizuho; Tohoku University, Department of Applied Chemistry, School of Engineering Osuga, Ryota; Tohoku University, Institute of Multidisciplinary Research for Advanced Materials Muramatsu, Atsushi; Tohoku University, Institute of Multidisciplinary Research for Advanced Materials; Tohoku University, International Center for Synchrotron Radiation Innovation Smart; Japan Science and Technology Agency, Core Research for Evolutional Science and Technology

Control of Location and Distribution of Heteroatoms Substituted Isomorphously in Framework of Zeolites and Zeotype Materials

Mizuho Yabushita,[a,*] Ryota Osuga,[b] Atsushi Muramatsu[b,c,d,*]

[a]Department of Applied Chemistry, School of Engineering, Tohoku University, 6-6-07 Aoba, Aramaki, Aoba-ku, Sendai, Miyagi 980-8579, Japan

[b]Institute of Multidisciplinary Research for Advanced Materials, Tohoku University, 2-1-1 Katahira, Aoba-ku, Sendai, Miyagi 980-8577, Japan

[c]International Center for Synchrotron Radiation Innovation Smart, Tohoku University, 2-1-1 Katahira, Aoba-ku, Sendai, Miyagi 980-8577, Japan

[d]Core Research for Evolutional Science and Technology, Japan Science and Technology Agency, 4-1-8 Honcho, Kawaguchi, Saitama 332-0012, Japan

**Corresponding authors: m.yabushita@tohoku.ac.jp (M.Y.); mura@tohoku.ac.jp (A.M.)*

ABSTRACT

Zeolites and zeotype materials, which are porous and crystalline metallosilicates, are key functional materials widely used as adsorbents and catalysts in the chemical industry. The function and performance of these materials are significantly dependent on heteroatoms that substitute isomorphously the tetrahedral sites, so-called the T-sites, of the frameworks. In addition to the types of substituting heteroatoms, their location and distribution in frameworks also dominate the performance of zeolites and zeotype materials as adsorbents and catalysts; for example, the acid sites generated on substituting Al^{3+} for Si^{4+} in the channels and at the channel intersections of **MFI**-type zeolites exhibit different catalytic activities for some reactions. In this context, the development of a synthetic procedure to control isomorphous substitution by heteroatoms with precision is highly desired. This highlight introduces recent achievements related to such precise tuning of the location and distribution of substituting heteroatoms, mainly Al^{3+}, by a variety of synthetic approaches along with the effects of such well-controlled heteroatom siting on catalytic performance.

1. Introduction

The unique and attractive properties of zeolites and zeotype materials—their crystalline framework, microporous (and sometimes mesoporous) characteristics, high thermal stability, acidity, and ion-exchange properties—have made them central materials in a variety of research fields for decades.[1–7] The most important application of these materials is their catalytic use in the chemical

industry, namely petroleum refining processes including fluid catalytic cracking, upgrading, and dewaxing.[1–8] Among the properties listed above, the acidity and ion-exchange properties of zeolites and zeotype materials impact greatly on their catalytic performance and are tunable via isomorphous substitution on tetrahedral sites (so-called T-sites) of the framework, which are originally occupied by Si^{4+}, by heteroatoms. As exemplified by the **MFI**-type metallosilicates in which Si^{4+} is substituted by trivalent cations (*i.e.*, B^{3+}, Al^{3+}, Fe^{3+}, and Ga^{3+}) and H^{+} is involved for charge balance in the negatively charged framework, they exhibit Brønsted acidity, and the order of their acid strength has been demonstrated experimentally to be [B]-MFI << [Fe]-MFI < [Ga]-MFI < [Al]-MFI (in this paper, [M]-MFI represents an **MFI**-type framework with isomorphous substitution by "M" elements),[9] which has also been confirmed via density functional theory (DFT) calculations.[10,11] When Si^{4+} is substituted by tetravalent cations like Sn^{4+}, such zeotype materials are known to function as Lewis acid catalysts.[12,13] Given that the acid-site density and ion-exchange capacity are correlated with the degree of framework substitution, the performance of zeolites and zeotype materials as catalysts and adsorbents is dependent on the type and amount of substituting heteroatoms.

Other crucial parameters with respect to isomorphous substitution by heteroatoms are their location and distribution in the frameworks of zeolites and zeotype materials, which govern catalytic activity and selectivity as well as ion-exchange properties of these materials, since the accessibility of substrate molecules toward active sites consisting of substituting heteroatoms and/or neighboring

charge-compensating ions is of importance. For instance, any substrate molecules can interact with such sites present on the outer surface, while only molecules smaller than the pore size are allowed to gain access to catalytic sites on the inner surface.[14,15] Likewise, as seen in topologies like **FAU** and **MFI**, some frameworks consist of cages and/or channel intersections, and such wide spaces with catalytic sites derived from heteroatom substitution allow substrate molecules to form transition state species with large steric hindrance that cannot be formed in narrow channels; in stark contrast, substituting heteroatoms located in narrow channels only support reactions involving transition states with small steric hindrance. Therefore, selective siting of heteroatoms in frameworks offers a promising opportunity for selective production of desired products in catalytic reactions. Another important aspect to controlling the distribution of heteroatoms arises from the desire to develop single-atom catalysts, which maximize the atom efficiency of active heteroatoms, compared to a non-uniform structure including agglomerates of heteroatoms.[16–18] Such an uneven distribution of heteroatoms makes gaining an understanding of structures and functions extremely difficult, and what is worse, sometimes triggers undesired issues (*e.g.*, byproduct formation in catalytic reactions).[16–18] Therefore, the location and distribution of heteroatoms in zeolites and zeotype materials need to be controlled precisely for each desired application. In the following sections, we highlight various strategies for achieving such fine tuning of heteroatom substitution and the unique catalytic performance of the resulting zeolites and zeotype materials.

2. Control of Al locations in channels and/or intersections

The first approach introduced in this highlight on controlling the location of heteroatoms relies on the bulkiness of positively charged structure-directing agents (SDAs), which attract negatively charged trivalent heteroatom-containing building blocks (*i.e.*, polymetallosilicates) via electrostatic interaction during hydrothermal processes. Bulky SDA molecules like tetraalkylammonium cations cannot enter into narrow pores but are accommodated in wide spaces such as cages and channel intersections, resulting in the formation of substituting heteroatoms that face wide spaces. In stark contrast, small SDAs like Na^+ are taken into both narrow and wide spaces, leading to a random distribution of substituting heteroatoms in channels, cages, and intersections. Based on such insights on SDAs, the effects of SDAs on the location of Al, which is the most common substituting element for zeolite frameworks, have been investigated intensively. Yokoi *et al.* demonstrated that the location of Al atoms involved in the **MFI**-type framework is altered by using tetra-*n*-propylammonium cations (TPA^+) alone or a combination of TPA^+ and Na^+, both of which are typical SDAs for synthesizing **MFI**-type zeolites.[19] In the former case, due to the bulkiness of TPA^+, all Al atoms are present at the intersections of straight and sinusoidal channels (Fig. 1B); in contrast, the co-presence of Na^+ with TPA^+ allows Al atoms to become located in both at the intersections and in channels (Fig. 1A). Such Al locations were confirmed by high-resolution solid-state ^{27}Al magic angle spinning nuclear magnetic resonance (^{27}Al MAS NMR) spectroscopy and catalytic cracking

reactions with small and large hydrocarbon substrates consisting of *n*-hexane and 3-methylpentane. In the cracking reaction of *n*-hexane, its transition state with small steric hindrance is allowed to be formed even in the narrow channels of the **MFI** framework as well as at the wide intersections. As a result, [Al]-MFI zeolites synthesized hydrothermally in the presence of TPA^+ with/without Na^+ exhibited comparable catalytic performance to each other. On the other hand, for 3-methylpentane, which requires a wider space in the cracking reaction due to its transition state with large steric hindrance, [Al]-MFI zeolites containing only Brønsted acid sites located at intersections showed higher activity than those containing acid sites distributed both in channels and at intersections.

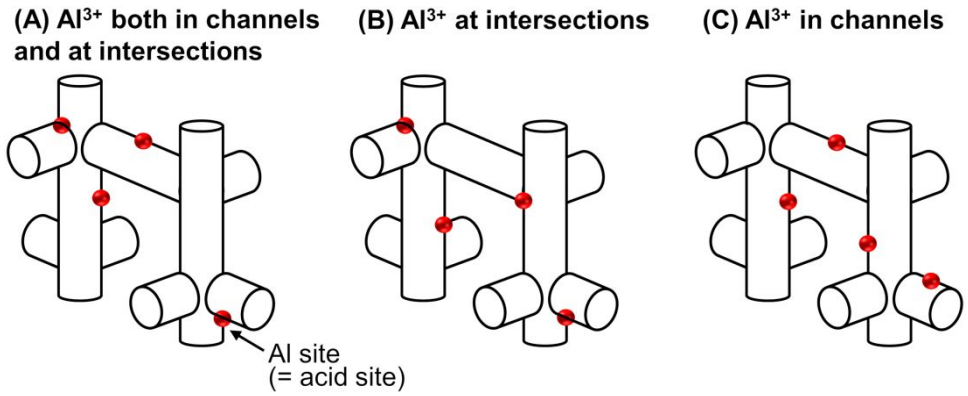

Fig. 1 Control of Al location in **MFI**-type zeolites.

The opposite distribution of Al species in the **MFI** framework (*i.e.*, Al atoms located in channels rather than at intersections, see Fig. 1C) was achieved via a two-step approach reported by Boronat and Corma *et al.*[20] In the first step, **MFI**-type zeolites with isomorphous substitution by both B and Al ([B, Al]-MFI) were synthesized hydrothermally. The DFT calculations demonstrated that B atoms

prefer to occupy the T-sites facing the intersections rather than those in the channels. Therefore, the co-presence of B and Al in the same synthesis gels led to B and Al atoms being located preferentially at the intersections and in channels, respectively. The post-synthetic treatment to remove B atoms (*i.e.*, deboronation) for the thus-prepared [B, Al]-MFI as a second step resulted in the selective location of Al atoms in the channels of the **MFI**-type framework. Compared to a typical [Al]-MFI containing randomly distributed Al atoms, the deboronated sample containing Al atoms in the channels exhibited higher propene selectivity in both the 1-hexene cracking and methanol-to-olefins (MTO) reactions. A different technique to place Al^{3+} in the channels of the **MFI**-type framework reported by Yokoi *et al.* relied on the simultaneous use of Na^{+} and pentaerythritol as SDAs.[21] In this system, a bulky pentaerythritol molecule acts in the same manner as TPA^{+} (*vide supra*), but its neutral character does not allow it to attract negatively charged Al-containing building blocks. Meanwhile, small Na^{+} ions attract such building blocks, which results in the incorporation of Al^{3+} species into the **MFI**-type framework facing the straight and sinusoidal channels rather than the intersections. The thus-prepared **MFI** zeolite containing Al^{3+} only in its channels exhibited a longer catalyst lifetime in the MTO reaction, compared to **MFI** zeolites with uncontrolled Al^{3+} sites prepared as control materials. In a separate work, the same research group employed various neutral SDAs, whose structure can be seen in Fig. 2, to investigate the effects of their structure on the distribution of Al^{3+} species substituted in the **MFI** framework.[22] The location of Al^{3+} species was evaluated based on the constraint index (CI), which is defined as the ratio of the reaction rate

constant for *n*-hexane cracking to that for 3-methylpentane cracking,[23] and reflects the distribution of Al^{3+};[19,21] that is, an **MFI**-type zeolite that provides a higher CI value contains a smaller amount of Al^{3+} species at the intersections and a greater amount in the channels. It is worth mentioning that if a suitable combination of substrate molecules with different bulkiness is selected carefully, the concept of CI should be applicable to other types of zeolite topologies to identify the location of substituting elements. Fig. 2 summarizes the evaluated CI values for **MFI** zeolites synthesized hydrothermally in the presence of various SDAs. The benchmark **MFI**-type zeolite, which was synthesized hydrothermally in the presence of Na^+ alone and thus contained Al^{3+} located both in channels and at intersections, exhibited a CI value of 6.7. The **MFI** zeolite synthesized in the presence of TPA^+ alone provided the lowest CI value of 2.3, indicating the presence of Al^{3+} species at the intersections (*vide supra*).[19] The co-presence of Na^+ and a neutral straight-chain SDA such as 1,3-propanediol or 1,6-hexanediol produced **MFI**-type zeolites that showed relatively low CI values, suggesting that Al^{3+} species were still located preferentially at the intersections. In contrast, the combination of Na^+ and a neutral bulky SDA such as pentaerythritol, *tert*-butyl alcohol, or trimethylolethane led to high CI values, indicating that Al^{3+} species were present mainly in the channels. Cheng *et al.* also compared the catalytic activity of **MFI** zeolites synthesized with TPA^+ and pentaerythritol in the aromatization of ethane after the impregnation of Pt on each catalyst surface.[24] The total yield of benzene, toluene, and xylene (BTX), all of which are typical products of the ethane aromatization, produced by a Pt-modified **MFI** zeolite synthesized using pentaerythritol decreased gradually from the beginning of

the reaction and became less than 10% within 150 min. In stark contrast, a Pt-modified **MFI** zeolite prepared with TPA^+ maintained a good BTX yield of *ca.* 35% even after 300 min. Given the fact that hydrogen transfer reactions, which are important steps in ethane aromatization and accelerated by acid sites, involve bulky intermediates, acid sites located in wider spaces are suitable for this reaction. Therefore, **MFI** zeolites containing Al^{3+} species mainly at the intersections exhibited better catalytic performance. Such preferential siting of Al^{3+} in the channels or at the intersections of **MFI** zeolites was also reported to impact on other catalytic reactions, such as the alkylation of benzene with methanol[25] and the cracking and dehydrogenation of *n*-butane[26].

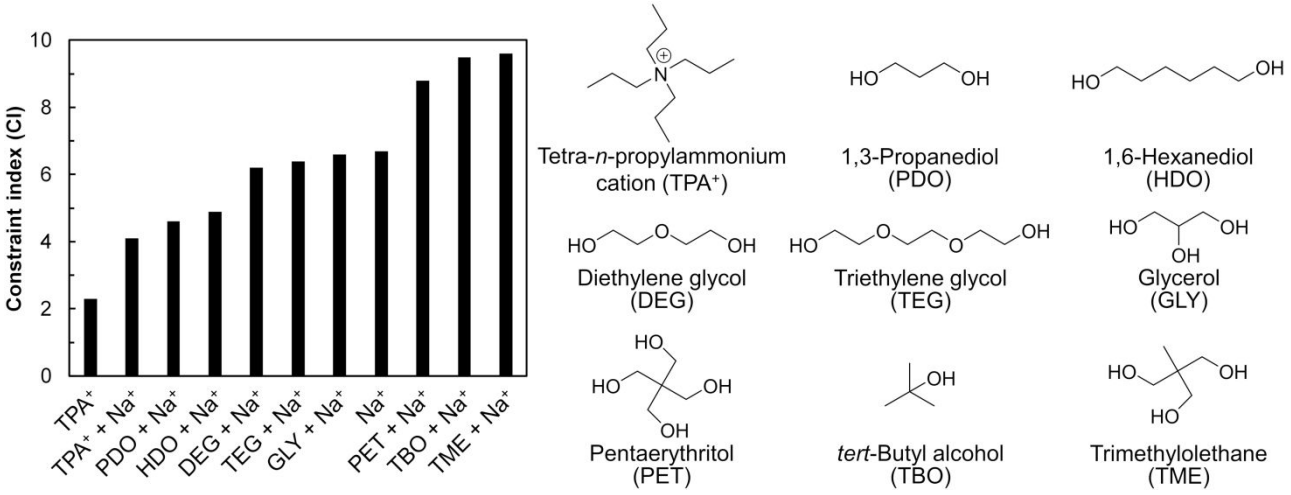

Fig. 2 Effect of SDAs on the constraint index (CI) for **MFI**-type zeolite catalysts. The data were taken from Ref. 22.

For the **MEL**-type topology, which has a three-dimensional porous structure similar to **MFI**,[27] tuning of the Al^{3+} population in the channels and at the intersections is possible by appropriately

adjusting the content of Na^+ and/or Li^+ in addition to the Si/Al ratio in the synthesis gels.[28] The Al^{3+} population at the intersections was enriched by adding Na^+ and/or Li^+ in the synthesis gels, while under alkali-ion-free conditions, increasing the Si/Al ratio enhanced the Al^{3+} content in the channels rather than at the intersections. In the MTO reaction, the **MEL** zeolites enriched with Al^{3+} in the channels produced small olefins like propene and butene as major products, whereas those containing Al^{3+} mainly at the intersections showed relatively higher selectivity toward BTX.

3. Uniform distribution of substituting heteroatoms achieved by using mixed-oxide precursors

The second scenario in this highlight aims to achieve uniform dispersion of substituting heteroatoms over entire particles of zeolites and zeotype materials. For this purpose, the concentrations (more precisely, chemical potentials) of both the Si and heteroatom sources dissolved in the synthesis gels need to be kept constant throughout the hydrothermal process. In typical liquid-phase syntheses of materials, the chemical potentials of homogeneous starting reagents (for synthesizing zeolites and zeotype materials, tetraethyl orthosilicate (TEOS) and metal nitrates are typically employed) inevitably decrease during precipitation of solid products, and thus alter the kinetics of crystal growth,[29] leading to an uncontrolled, non-uniform distribution of heteroatoms in resulting materials. To avoid this situation, supplying the Si and substituting heteroatoms from solid precursors via solid-liquid equilibrium is a promising means of controlling the chemical potentials of Si and substituting heteroatoms such that they remain constant throughout the synthetic process,

because once the Si and heteroatom sources are consumed via precipitation to form the desired solid products (*i.e.*, zeolites and zeotype materials), solid precursors like SiO_2-based mixed oxides are partially dissolved to supply Si and heteroatom sources under the control of the solid-liquid equilibrium. Another important insight that needs to be considered carefully is the difference in the condensation rates (*i.e.*, olation and oxolation)[30] for Si and heteroatom species, which leads to a non-uniform distribution of heteroatoms in the resulting zeolites and zeotype materials. In this context, the preparation of suitable solid precursors is a key step to achieving a uniform distribution of heteroatoms in resulting zeolites and zeotype materials.

A mechanochemical approach pioneered by Yamamoto *et al.* provides desirable solid precursors for zeolites and zeotype materials (Fig. 3).[31–36] In this method, SiO_2 and a source for the substituting heteroatoms (*e.g.*, metal oxide, metal hydroxide, or metal oxyhydroxide) are pulverized together via planetary ball-milling to induce a mechanochemical reaction at the interface of these solid materials, resulting in the formation of amorphous metallosilicates. In a subsequent hydrothermal process using the thus-prepared amorphous metallosilicates, polymetallosilicates are dissolved from the amorphous metallosilicates under the control of the solid-liquid equilibrium and then crystallized and precipitated as zeolites and zeotype materials.[32,37–40] Another benefit of the use of metallosilicates as starting reagents for hydrothermal processes arises from the preformed Si–O–metal species, which enable one to ignore the difference in condensation rates between Si and heteroatoms species.

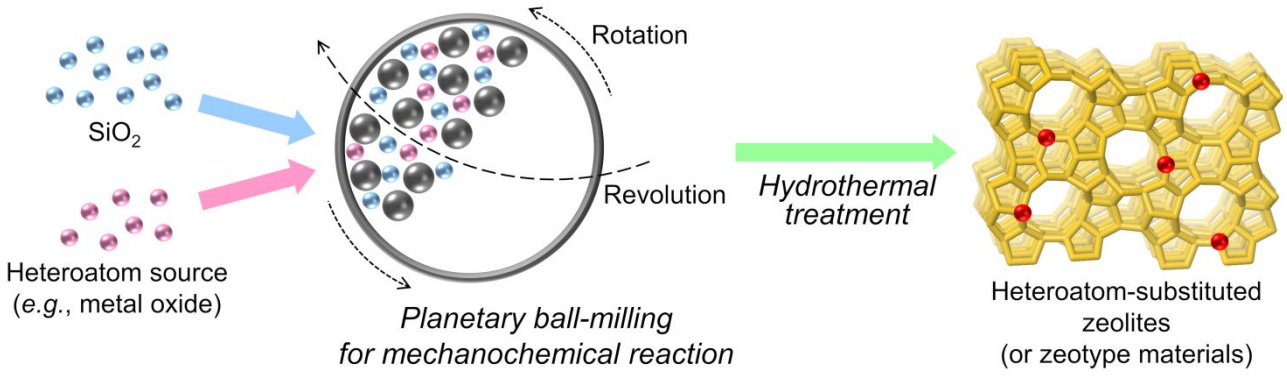

Fig. 3 Schematic of mechanochemical method.

We recently succeeded in the syntheses of the **MFI**-type zeolites with isomorphous substitution by both Al and Fe atoms ([Al, Fe]-MFI) from the mechanochemical preparation of two different amorphous metallosilicates, aluminosilicates and ferrisilicates (the thus-prepared zeolite sample is denoted hereafter as [Al, Fe]-MFI_{MC}).[41] The ultraviolet-visible (UV-vis) spectrum of [Al, Fe]-MFI_{MC} with Si/Al and Si/Fe ratios of 200 and 50, respectively, exhibited a narrower absorption band, compared to a control material synthesized from TEOS, $Al(NO_3)_3$, and $Fe(NO_3)_3$ (denoted as [Al, Fe]-MFI_{HT}),[42] which gave a broader band in the range from 200 to 450 nm (Fig. 4A). This difference in the UV-vis spectra demonstrated that tetrahedral Fe species—which could be incorporated in the framework—were formed in [Al, Fe]-MFI_{MC}, yet in addition to such species, more aggregated Fe species like FeO_x clusters and bulk Fe oxides were present outside the framework in [Al, Fe]-MFI_{HT}. These two [Al, Fe]-MFI zeolites exhibited different catalyst lifetimes in the dimethyl ether-to-olefins (DTO) reaction (Fig. 4B). [Al, Fe]-MFI_{MC} maintained its catalytic performance (*i.e.*, conversion of dimethyl ether and selectivity toward light olefins consisting of ethene, propene, and butene) longer

than [Al, Fe]-MFI_{HT}, clearly demonstrating the advantage of a uniform distribution of substituting elements in zeolite frameworks achieved by the mechanochemical approach.

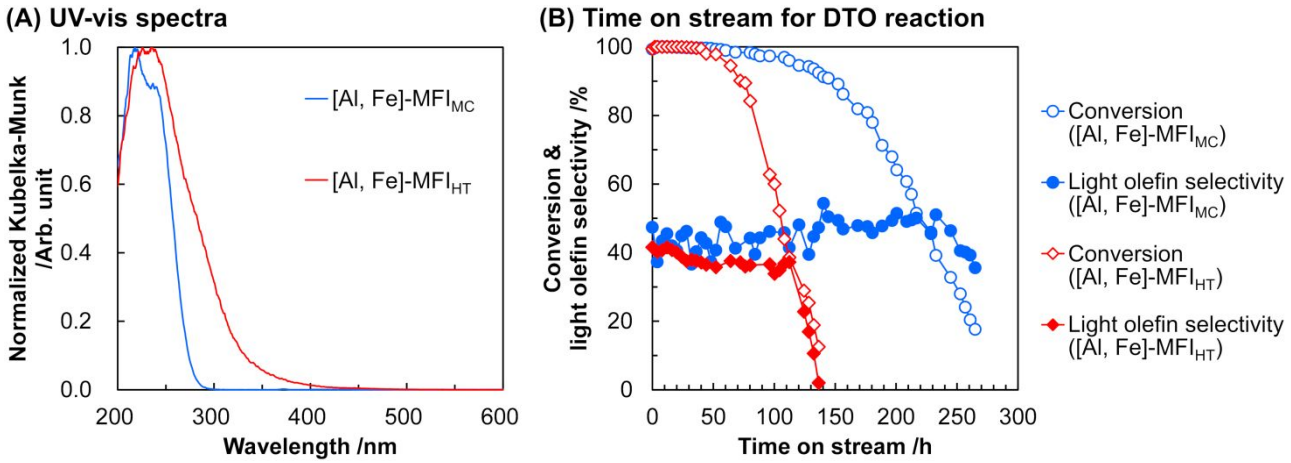

Fig. 4 (A) Nature of Fe species in [Al, Fe]-MFI_{MC} and [Al, Fe]-MFI_{HT}, confirmed by UV-vis spectroscopy. (B) Difference in catalyst lifetimes of [Al, Fe]-MFI_{MC} and [Al, Fe]-MFI_{HT} in the DTO reaction. Reaction conditions: catalyst 200 mg (mixed with 840 mg of quartz sand); 450 °C; W/F = 5.8 g h mol^{-1}. The data were taken from Ref. 41.

Likewise, a mechanochemically assisted preparation starting from SiO_2 and β-Ga_2O_3 provided unique **MFI**-type gallosilicates ([Ga]-MFI_{MC}), which exhibited completely different catalytic activity from a control material synthesized by the conventional one-pot hydrothermal process using SiO_2 and $Ga(NO_3)_3$ ([Ga]-MFI_{HT}).[43] In the oxidative conversion of methane, [Ga]-MFI_{MC} yielded CO at up to 80% selectivity with 20% selectivity of CO_2 at 650 °C; in stark contrast, [Ga]-MFI_{HT} instead produced CO_2 as the major product at up to 94% selectivity with 6% selectivity of CO under the

same reaction conditions. As introduced here, the use of amorphous metallosilicates as starting reagents in hydrothermal processes offers an opportunity to synthesize unique and attractive zeolite catalysts that cannot be produced from homogeneous reagents.

4. Conclusions and outlook

Through choice of the proper synthetic techniques, it is possible to control the distribution and location of heteroatoms substituting isomorphously into the frameworks of zeolites and zeotype materials. Bulky SDAs attract negatively charged building blocks containing heteroatoms to only wide spaces such as cages and intersections, while small SDAs attract heteroatoms to both wide and narrow spaces. Post-synthesis treatment is also a promising approach to the placement of heteroatoms at desired locations. The use of solid metallosilicates as precursors for hydrothermal processes enables to the synthesis of zeolites and zeotype materials that contain substituting heteroatoms distributed uniformly. Such controlled heteroatoms offer unique catalytic performance for a variety of reactions that cannot be achieved by the uncontrolled hydrothermal processes.

A grand challenge for zeolite chemistry is more precise, atomic-level control of heteroatom positions in frameworks, compared to the examples introduced above. A variety of framework topologies possess multiple crystallographically distinct T-sites. For instance, the **MFI**-type framework has 12 T-sites,[27] and electronic structure calculations have demonstrated that the stability of Al species involved in these T-sites differs.[44,45] This stability difference leads to a preference for

Al siting at specific T-sites in the resulting materials to gain a thermodynamic advantage, rather than completely random Al siting at any T-site, which was confirmed experimentally by high-resolution two-dimensional ^{27}Al multiple-quantum/MAS NMR spectroscopy for a variety of framework topologies as exemplified by **FER**,[46] **MEL**,[47] **MFI**,[47] and **MWW**[48]. However, such a thermodynamic preference is not sufficient to incorporate Al atoms only at designated T-sites. Given the fact that the positions of Al atoms (*i.e.*, T-sites) were also demonstrated to impact on Brønsted acidity (*i.e.*, strength) by electronic structure calculations[10,45,49]—for example, in the case of [Al]-MFI, the most stable Al-substituted T-site exhibited the highest affinity for H^+ as a counter cation and its affinity differed by 29 kJ mol^{-1} from the worst one[45]—the development of synthetic techniques capable of selective incorporation of heteroatoms into desired T-sites is an attractive means of providing well-tuned zeolites and zeotype materials. For the **IFR**-type zeolites, the occupancy of Al atoms at four different crystallographically distinct T-sites was tuned successfully by using three different organic SDA molecules as illustrated in Fig. 5.[50]

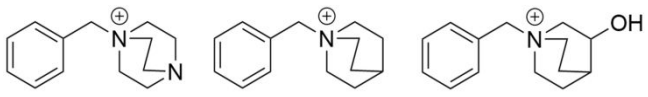

Fig. 5 Organic SDA molecules used for tuning the occupancy of Al atoms at four crystallographically different T-sites of **IFR**-type zeolites.

The selective placement of Sn species in specific T-sites in the **BEC**-type framework, which possesses three crystallographically different T-sites with two of them being involved in the double-4-ring (D4R) secondary building units,[27] was recently achieved by Román-Leshkov and Moliner *et al*. via a multi-step synthetic procedure (Fig. 6).[51] This strategy is based on the fact that Ge species are likely to occupy the T-sites in the D4Rs.[52,53] The initial step of this procedure was the synthesis of **BEC** germanosilicate at a high Si/Ge ratio (> 150), resulting in the preferential siting of Ge species at the T-sites of the D4R. Degermanation of this [Ge]-BEC generated defect sites, into which Sn species were successfully installed. The thus-prepared [Sn]-BEC possessing Sn species in the D4Rs exhibited a higher per-gram reaction rate in the Meerwein–Ponndorf–Verley–Oppenauer (MPVO) reaction using 2-butanol and cyclohexanone as substrates, due to its larger number of open Sn sites that can function as Lewis acid sites, compared to a conventional [Sn]-BEA catalyst.

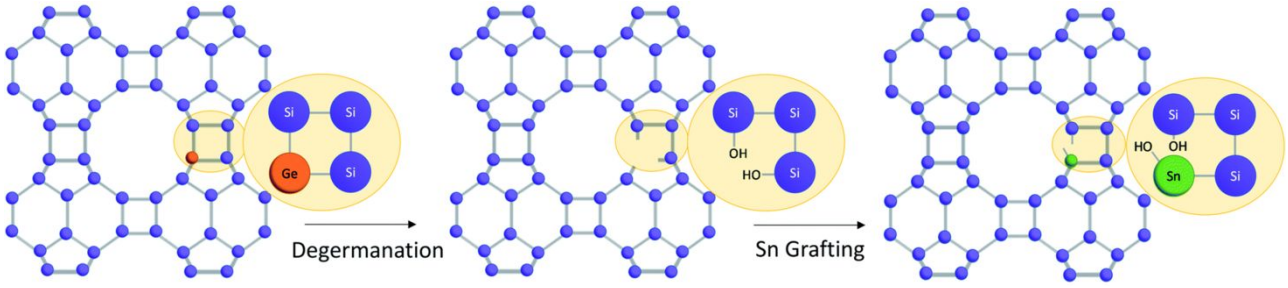

Fig. 6 Selective incorporation of Sn at the T-sites involved in D4Rs of a **BEC**-type framework via a multi-step synthetic method. Reproduced from Ref. 51 with permission from the Royal Society of Chemistry, copyright 2020.

Another hot topic with respect to atomic-level control of heteroatom positions in zeolites and zeotype materials is the incorporation of two Al atoms in proximity to each other. The motivation to incorporate two Al atoms at a close distance has arisen from the desire to create ion-exchange sites capable of capturing divalent cationic species, which function as catalytic active sites. Due to the widely accepted limitation known as Loewenstein's rule, which forbids the formation of nearest neighboring Al atoms (*i.e.*, Al–O–Al sequence) due to the instability of this configuration,[54] so-called Al pair sites referred to as Al–O–(Si–O)$_n$–Al (n = 1 or 2) sequences are possible juxtaposed structures in zeolite frameworks. Although the pairing possibility increases automatically at low Si/Al ratios, strategic synthesis methods enabling the formation of such paired Al sites even at high Si/Al ratios need to be devised. Dědeček *et al.* reported that the Al sources employed for the hydrothermal process significantly impacted on the ratio of paired Al atoms to isolated Al atoms in the resulting **MFI**-type zeolites; among the Al sources tested (*i.e.*, $AlCl_3$, $Al(OH)_3$, $Al(NO_3)_3$, and aluminum tri-*sec*-butoxide), $AlCl_3$ gave the highest content of paired Al sites.[55] For characterization of such paired Al species, the ion exchange technique combined with UV-vis spectroscopy using Co^{2+} as a probe is typically employed,[56] along with solid-state ^{29}Si MAS NMR spectroscopy, which detects Al–O–Si–O–Al sequences directly as a peak of Q^4(2Al) but cannot detect another Al-paired sequence, Al–O–(Si–O)$_2$–Al. The Si sources also affected the ratio of paired to isolated Al species, but their effect was not as great as that caused by the Al sources.[55] In a detailed study by the same research group, they succeeded in varying the percentage of Al involved in Al–O–(Si–O)$_2$–Al

sequences in the range of 6–66% by altering the composition of the synthesis gels, where both van der Waals and electrostatic interactions play key roles in controlling the paired Al content.[57] For the **CHA**-type topology, Di Iorio and Gounder demonstrated the combination of two SDAs, Na^+ and *N*,*N*,*N*-trimethyl-1-adamantylammonium cation ($TMAda^+$), the latter of which is necessary for construction of the **CHA**-type framework, to be effective at forming Al pair sites.[58] A lack of Na^+ in the synthesis gel instead provided isolated Al sites in the **CHA** framework. This difference can be rationalized by the size of the SDAs. The presence of only $TMAda^+$ in the synthesis gel did not allow paired Al sites to form due to its bulky structure, while the co-presence of small Na^+ with $TMAda^+$ enabled the generation of those sites (Fig. 7). In a separate study, the same group found that the co-presence of K^+, which is larger than Na^+, did not work well for the formation of paired Al sites in **CHA**.[59] Yokoi *et al.* considered a different strategy for generating paired Al sites in **CHA**-type zeolites.[60] In their approach, an **FAU**-type zeolite with a Si/Al ratio of 2.8, in which paired Al sites were generated automatically owing to its high Al content, was used as a starting reagent, from which building blocks containing paired Al species were first dissolved into a liquid phase and then precipitated; in other words, the paired Al species originally present in the **FAU**-type zeolite were transferred into the resulting **CHA** products. In stark contrast, the combination of SiO_2 and $Al(NO_3)_3$, which lacked pre-formed Al pairs, provided **CHA** zeolites rich in isolated Al. In addition to the examples introduced here, a variety of techniques to form paired Al sites in some framework topologies have also been reported and summarized in excellent review papers.[61,62]

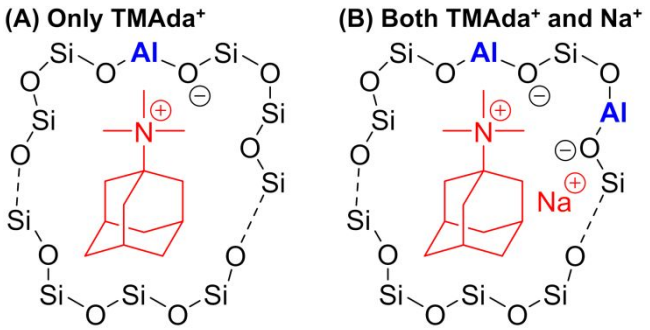

Fig. 7 Proposed organization of sources of Si and Al, $TMAda^+$, and Na^+ in synthesis gels during hydrothermal processes: (A) **CHA** synthesis with only $TMAda^+$ to provide single Al sites and (B) **CHA** synthesis with both $TMAda^+$ and Na^+ to form paired Al sites.

Altogether, various excellent approaches have enabled control of the positions of substituting heteroatoms even at the atomic level for some framework topologies. Meanwhile, all the examples introduced above are applicable to specific topologies, yet more than 200 types of zeolite framework topologies have been approved thus far in the database provided by the International Zeolite Association (IZA).[27] In this respect, the development of more widely applicable means (ultimately, those enabling the precise control of heteroatom positions for all framework topologies), which will open the door to accessing outstanding functional materials, remains an enormous challenge. Given the fact that construction of desired framework topology requires corresponding SDA(s), for example, the present means of controlling location and distribution of heteroatoms in **MFI**-type zeolites that rely on the use of the specific SDA(s) (see Section 2) are not directly applicable to the synthesis of other framework topologies with position-controlled substituting heteroatoms. To solve this dilemma, a deep insight on the structural properties of each SDA is necessary. Molecular

dynamics simulations, which previously enabled the rational discovery of SDA(s),[63,64] should assist in tackling such a grand challenge; furthermore, from the viewpoint of practical applications of synthesized zeolites and zeotype materials, computational simulation would also predict cost-effective SDA(s).[65] Along with such approaches, advanced characterization techniques that have not yet been used widely in the field of zeolite chemistry thus far—for example, pair distribution function (PDF) analysis,[66,67] diffraction anomalous fine structure (DAFS; combination of X-ray diffraction (XRD) and X-ray absorption spectroscopy (XAS)), X-ray standing wave (XSW) analysis,[68] and X-ray ptychography[69]—could offer great opportunities for forming a deep understanding of the local environment of substituted heteroatoms, in addition to conventional approaches such as XRD, NMR spectroscopy, X-ray photoelectron spectroscopy (XPS), Fourier transformed infrared (FT-IR) spectroscopy, UV-vis spectroscopy, and electron microscopy.

Conflicts of interest

There are no conflicts to declare.

Acknowledgements

This work was supported financially by Core Research for Evolutional Science and Technology of the Japan Science and Technology Agency (JST CREST, Grant No. JPMJCR16P3) and a Grant-in-

Aid for Scientific Research (S) (KAKENHI, 21H05011) from the Japan Society for the Promotion of Science (JSPS).

References

1 J. Čejka, A. Corma and S. Zones, *Zeolites and catalysis: synthesis, reactions and applications*, Wiley-VCH, Weinheim, 2010.

2 T. Ennaert, J. Geboers, E. Gobechiya, C. M. Courtin, M. Kurttepeli, K. Houthoofd, C. E. A. Kirschhock, P. C. M. M. Magusin, S. Bals, P. A. Jacobs and B. F. Sels, *ACS Catal.*, 2015, **5**, 754–768.

3 Y. Li, L. Li and J. Yu, *Chem*, 2017, **3**, 928–949.

4 M. Dusselier and M. E. Davis, *Chem. Rev.*, 2018, **118**, 5265–5329.

5 J. Přech, P. Pizarro, D. P. Serrano and J. Čejka, *Chem. Soc. Rev.*, 2018, **47**, 8263–8306.

6 A. Deneyer, Q. Ke, J. Devos and M. Dusselier, *Chem. Mater.*, 2020, **32**, 4884–4919.

7 T. T. Le, A. Chawla and J. D. Rimer, *J. Catal.*, 2020, **391**, 56–68.

8 T. F. Degnan Jr., *Top. Catal.*, 2000, **13**, 349–356.

9 C. T. W. Chu and C. D. Chang, *J. Phys. Chem.*, 1985, **89**, 1569–1571.

10 M. S. Stave and J. B. Nicholas, *J. Phys. Chem.*, 1995, **99**, 15046–15061.

11 A. Chatterjee, T. Iwasaki, T. Ebina and A. Miyamoto, *Microporous Mesoporous Mater.*, 1998, **21**, 421–428.

12 Y. Román-Leshkov, M. Moliner, J. A. Labinger and M. E. Davis, *Angew. Chem. Int. Ed.*, 2010, **49**, 8954–8957.

13 R. Bermejo-Deval, M. Orazov, R. Gounder, S.-J. Hwang and M. E. Davis, *ACS Catal.*, 2014, **4**, 2288–2297.

14 S. M. Csicsery, *Zeolites*, 1984, **4**, 202–213.

15 B. Smit and T. L. M. Maesen, *Nature*, 2008, **451**, 671–678.

16 X.-F. Yang, A. Wang, B. Qiao, J. Li, J. Liu and T. Zhang, *Acc. Chem. Res.*, 2013, **46**, 1740–1748.

17 J. Liu, *ACS Catal.*, 2017, **7**, 34–59.

18 Y. Chen, S. Ji, C. Chen, Q. Peng, D. Wang and Y. Li, *Joule*, 2018, **2**, 1242–1264.

19 T. Yokoi, H. Mochizuki, S. Namba, J. N. Kondo and T. Tatsumi, *J. Phys. Chem. C*, 2015, **119**, 15303–15315.

20 C. Li, A. Vidal-Moya, P. J. Miguel, J. Dedecek, M. Boronat and A. Corma, *ACS Catal.*, 2018, **8**, 7688–7697.

21 T. Yokoi, H. Mochizuki, T. Biligetu, Y. Wang and T. Tatsumi, *Chem. Lett.*, 2017, **46**, 798–800.

22 T. Biligetu, Y. Wang, T. Nishitoba, R. Otomo, S. Park, H. Mochizuki, J. N. Kondo, T. Tatsumi and T. Yokoi, *J. Catal.*, 2017, **353**, 1–10.

23 V. J. Frillette, W. O. Haag and R. M. Lago, *J. Catal.*, **67**, 218–222.

24 H. Liu, H. Wang, A.-H. Xing and J.-H. Cheng, *J. Phys. Chem. C*, 2019, **123**, 15637–15647.

25 Y. Wang, X. He, F. Yang, Z. Su and X. Zhu, *Ind. Eng. Chem. Res.*, 2020, **59**, 13420–13427.

26 A. Janda and A. T. Bell, *J. Am. Chem. Soc.*, 2013, **135**, 19193–19207.

27 C. Baerlocher and L. B. McCusker, Database of Zeolite Structures, http://www.iza-structure.org/databases/, (accessed July 2021).
28 S. Wang, L. Zhang, S. Li, Z. Qin, D. Shi, S. He, K. Yuan, P. Wang, T.-S. Zhao, S. Fan, M. Dong, J. Li, W. Fan and J. Wang, *J. Catal.*, 2019, **377**, 81–97.
29 T. Ly, J. Wen and L. D. Marks, *Nano Lett.*, 2018, **18**, 5186–5191.
30 J. Livage, *Catal. Today*, 1998, **41**, 3–19.
31 K. Yamamoto, S. E. B. Garcia, F. Saito and A. Muramatsu, *Chem. Lett.*, 2006, **35**, 570–571.
32 K. Yamamoto, S. E. B. García and A. Muramatsu, *Microporous Mesoporous Mater.*, 2007, **101**, 90–96.
33 S. E. B. Garcia, K. Yamamoto and A. Muramatsu, *J. Mater. Sci.*, 2008, **43**, 2367–2371.
34 K. Yamamoto, T. Ikeda, C. Ideta and M. Yasuda, *Cryst. Growth Des.*, 2012, **12**, 1354–1361.
35 K. Kanie, M. Sakaguchi, F. Muto, M. Horie, M. Nakaya, T. Yokoi and A. Muramatsu, *Sci. Technol. Adv. Mater.*, 2018, **19**, 545–553.
36 M. Yabushita, M. Yoshida, R. Osuga, F. Muto, S. Iguchi, S. Yasuda, A. Neya, M. Horie, S. Maki, K. Kanie, I. Yamanaka, T. Yokoi and A. Muramatsu, *Ind. Eng. Chem. Res.*, 2021, DOI: 10.1021/acs.iecr.1c01664.
37 C. S. Cundy and P. A. Cox, *Chem. Rev.*, 2003, **103**, 663–702.
38 C. S. Cundy and P. A. Cox, *Microporous Mesoporous Mater.*, 2005, **82**, 1–78.
39 G. Majano, L. Borchardt, S. Mitchell, V. Valtchev and J. Pérez-Ramírez, *Microporous Mesoporous Mater.*, 2014, **194**, 106–114.
40 T. Xiao, M. Yabushita, T. Nishitoba, R. Osuga, M. Yoshida, M. Matsubara, S. Maki, K. Kanie, T. Yokoi, W. Cao and A. Muramatsu, *ACS Omega*, 2021, **6**, 5176–5182.
41 M. Yabushita, H. Kobayashi, R. Osuga, M. Nakaya, M. Matsubara, S. Maki, K. Kanie and A. Muramatsu, *Ind. Eng. Chem. Res.*, 2021, **60**, 2079–2088.
42 M. Yabushita, H. Kobayashi, A. Neya, M. Nakaya, S. Maki, M. Matsubara, K. Kanie and A. Muramatsu, *CrystEngComm*, 2020, **22**, 7556–7564.
43 M. Yabushita, M. Yoshida, F. Muto, M. Horie, Y. Kunitake, T. Nishitoba, S. Maki, K. Kanie, T. Yokoi and A. Muramatsu, *Mol. Catal.*, 2019, **478**, 110579.
44 S. R. Lonsinger, A. K. Chakraborty, D. N. Theodorou and A. T. Bell, *Catal. Lett.*, 1991, **11**, 209–217.
45 A. Redondo and P. J. Hay, *J. Phys. Chem.*, 1993, **97**, 11754–11761.
46 J. Dedecek, M. J. Lucero, C. Li, F. Gao, P. Klein, M. Urbanova, Z. Tvaruzkova, P. Sazama and S. Sklenak, *J. Phys. Chem. C*, 2011, **115**, 11056–11064.
47 S. Wang, P. Wang, Z. Qin, Y. Chen, M. Dong, J. Li, K. Zhang, P. Liu, J. Wang and W. Fan, *ACS Catal.*, 2018, **8**, 5485–5505.
48 Y. Wang, Y. Gao, S. Xie, S. Liu, F. Chen, W. Xin, X. Zhu, X. Li, N. Jiang and L. Xu, *Catal. Today*, 2018, **316**, 71–77.
49 A. Ghorbanpour, J. D. Rimer and L. C. Grabow, *Catal. Commun.*, 2014, **52**, 98–102.
50 K. Muraoka, W. Chaikittisilp, Y. Yanaba, T. Yoshikawa and T. Okubo, *Angew. Chem. Int. Ed.*, 2018, **57**, 3742–3746.
51 A. Rodríguez-Fernández, J. R. Di Iorio, C. Paris, M. Boronat, A. Corma, Y. Román-Leshkov and M. Moliner,

Chem. Sci., 2020, **11**, 10225–10235.

52 T. Blasco, A. Corma, M. J. Díaz-Cabañas, F. Rey, J. A. Vidal-Moya and C. M. Zicovich-Wilson, *J. Phys. Chem. B*, 2002, **106**, 2634–2642.

53 G. Sastre, J. A. Vidal-Moya, T. Blasco, J. Rius, J. L. Jordá, M. T. Navarro, F. Rey and A. Corma, *Angew. Chem. Int. Ed.*, 2002, **41**, 4722–4726.

54 W. Loewenstein, *Am. Mineral.*, 1954, **39**, 92–96.

55 V. Gábová, J. Dědeček and J. Čejka, *Chem. Commun.*, 2003, 1196–1197.

56 J. Dědeček, D. Kaucký, B. Wichterlová and O. Gonsiorová, *Phys. Chem. Chem. Phys.*, 2002, **4**, 5406–5413.

57 J. Dedecek, V. Balgová, V. Pashkova, P. Klein and B. Wichterlová, *Chem. Mater.*, 2012, **24**, 3231–3239.

58 J. R. Di Iorio and R. Gounder, *Chem. Mater.*, 2016, **28**, 2236–2247.

59 J. R. Di Iorio, S. Li, C. B. Jones, C. T. Nimlos, Y. Wang, E. Kunkes, V. Vattipalli, S. Prasad, A. Moini, W. F. Schneider and R. Gounder, *J. Am. Chem. Soc.*, 2020, **142**, 4807–4819.

60 T. Nishitoba, N. Yoshida, J. N. Kondo and T. Yokoi, *Ind. Eng. Chem. Res.*, 2018, **57**, 3914–3922.

61 J. Dědeček, Z. Sobalík and B. Wichterlová, *Catal. Rev.*, 2012, **54**, 135–223.

62 J. Dědeček, E. Tabor and S. Sklenak, *ChemSusChem*, 2019, **12**, 556–576.

63 T. M. Davis, A. T. Liu, C. M. Lew, D. Xie, A. I. Benin, S. Elomari, S. I. Zones and M. W. Deem, *Chem. Mater.*, 2016, **28**, 708–711.

64 S. K. Brand, J. E. Schmidt, M. W. Deem, F. Daeyaert, Y. Ma, O. Terasaki, M. Orazov and M. E. Davis, *Proc. Natl. Acad. Sci. U.S.A.*, 2017, **114**, 5101–5106.

65 R. Pophale, F. Daeyaert and M. W. Deem, *J. Mater. Chem. A*, 2013, **1**, 6750–6760.

66 H. Yamada, T. Iida, Z. Liu, Y. Naraki, K. Ohara, S. Kohara, T. Okubo and T. Wakihara, *Cryst. Growth Des.*, 2016, **16**, 3389–3394.

67 T. Iida, K. Ohara, Y. Román-Leshkov and T. Wakihara, *Phys. Chem. Chem. Phys.*, 2018, **20**, 7914–7919.

68 J. A. van Bokhoven, T.-L. Lee, M. Drakopoulos, C. Lamberti, S. Thieß and J. Zegenhagen, *Nat. Mater.*, 2008, **7**, 551–555.

69 T. Li, J. Ihli, Z. Ma, F. Krumeich and J. A. van Bokhoven, *J. Phys. Chem. C*, 2019, **123**, 8793–8801.